Unmixing Algorithms for the Identification of Radionuclide Signatures in the Presence of Natural Background and Shielded Materials

M. Weiss[a], M. Fang[a], Y. Altmann[b], A. Di Fulvio[a,*]

[a] *Department of Nuclear, Plasma, and Radiological Engineering, University of Illinois, Urbana-Champaign, 104 South Wright Street, Urbana, IL 61801, United States*

[b] *School of Engineering and Physical Sciences, Heriot-Watt University, Riccarton, Edinburgh, EH14 4AS, United Kingdom*

Abstract

National security relies on several layers of protection. One of the most important ones is the traffic control at borders and ports that exploits Radiation Portal Monitors (RPMs) to detect and deter potential smuggling attempts. Two relevant issues for the identification of radioactive materials at RPMs are the presence of natural background radiation and shielding materials surrounding the sources. In this paper, we study the robustness of the unmixing algorithm that we have developed for source identification in both cases: (1) gamma-ray bare source unmixing in the presence of natural background, and (2) identification of shielded neutron sources. Neutron sources are more difficult to shield than gamma-ray sources and therefore can be easier to detect during passive inspection. This would be a particularly challenging scenario for the unmixing algorithm because of the shielding material's ability to act as a spectrum modulator. For the first application, we experimentally studied the robustness of the unmixing algorithm to different radiation background spectra, due to varying atmospheric conditions, in the 16°C to 28°C temperature range. The unmixing algorithm can be used to reliably identify the unshielded gamma-ray radionuclides that triggered an alarm, even with fewer than 1,000 detected counts and in the presence of multiple nuclides at the same time. With fewer than 500 counts available, we found larger differences of approximately 35.9% between estimated nuclide fractions and actual ones. For the second application, we simulated a beryllium-reflected plutonium source shielded by various materials and studied the effect of the spectral modifications induced by shielding on the unmixing response. For shielded neutron source configurations, the algorithm requires as few as 5,000 counts in the whole spectrum to remain effective.

Keywords: radiation portal monitors, organic scintillators, unmixing, expectation propagation, shielding, background radiation

1. Background and Motivation

One of the greatest lines of defense to deter, detect, and interdict the illicit movement of special nuclear material (SNM) and radioactive sources is the application of radiation portal monitors (RPMs) at the country's many ports of entry [1]. RPMs are capable of detecting statistically significant increases in radiation above natural background. Radioactive sources that result in a count rate within the statistical uncertainty of the RPM, close to or below natural background, have zero chance of being picked up by RPMs. RPMs typically encompass plastic scintillators, e.g., polyvinyl-toluene (PVT), sensitive to gamma rays, and He-3 proportional counters or ^{6}LiZnS-based scintillators, sensitive to neutrons [2]. For most vehicle and rail RPMs, the use of plastic scintillator allows to cover very large solid angle at reasonable costs, thus achieving high efficiency. The prompt detection of radioactive sources must be performed in a short time window of a few seconds to keep traffic flowing properly. The performance of a portal monitor in terms of sensitivity, i.e., maximization of the positive detection rate, depends on the detection efficiency of the system and its form factor, which should be optimized for a specific application [3]. In previous studies [4], we experimentally demonstrated the use of a sparsity-promoting Bayesian algorithm capable of unmixing the signatures from weak gamma-ray sources, detected by organic scintillators. Our algorithm, hereafter referred to as the unmixing algorithm, allowed to identify radioactive sources based on measured spectra consisting of less than 500 counts despite the relatively low energy resolution featured by organic scintillators. In an unknown spectrum with approximately 1000 counts, the algorithm is able to identify up to three gamma emitting radionuclides. The algorithm relies on a pre-compiled library of radionuclides to correctly

*Corresponding author. Tel.: +1 (217) 300-3739
Email address: difulvio@illinois.edu (A. Di Fulvio)

identify the mixture components. The library encompassed the most common gamma-ray emitting nuclides among naturally-occurring radioactive material (NORM), laboratory gamma-ray sources, radio-isotopes for medical applications, and special nuclear materials. These materials can often cause nuisance alarms, which are false alarms that will slow down the flow of traffic at the RPM ports of entry. Source identification for neutron sources requires further expansion of a source library to include neutron sources that may also be attenuated by means of different shielding layers. The presence of background radiation can have a large impact on the detection sites, with cosmic and terrestrial radiation being seen on the detected spectra. In the inherently low signal-to-background measurement conditions at RPMs, the intrinsic observation noise should not be neglected and can be modeled as Poisson noise, i.e., shot noise.

In this study, we focus on extending the use of the sparsity-promoting Bayesian algorithms to identify multiple radionuclide sources in an unknown mixture in the presence of different background conditions, as well as identifying the shielding materials in a sparse SNM neutron measurement. The main difference between these implementations is that instead of only identifying which radiation source is present as in the gamma source identification, both the neutron source and its shielding component can be identified simultaneously when the difference from natural background radiation is detected. Performing the neutron source unmixing requires a slight modification to the algorithm to account for each shielding material's neutron cross sectional data. Previous works make use of the neutron interaction cross-sections of the various shielding materials and implement these into the calculation of the predicted neutron energy spectra [5]. In the work by Lawrence et al. [5], different shielding layers were tested and the spectra were unfolded by taking the cross section of each material into account when reconstructing an attenuated spectra incident on the detector with a known initial fission spectrum. This procedure allowed for the unfolding algorithm to estimate the thickness of a variety of highly explosive attenuating materials present in the shielding to within 10% of the true thickness. Our algorithm attempts to perform a similarly effective unmixing while using fewer overall counts to reconstruct the original spectra.

2. Methods

2.1. Experimental Methods

Background radiation, humidity, and temperature measurements were taken from an outdoor environment in Urbana, Illinois, US (40.1106° N, 88.2073° W). The detectors for the long-term radiation, temperature and humidity data gathering were housed in an outdoor shelving unit with the sides covered by a thin sheet of plastic to keep out rainfall. This approach prevented the inside of the shelving unit from becoming a micro-environment with a possibly different temperature and humidity than the outside. Changes in the background count rate could be the effect of three different causes: (1) the actual increase of the background radiation, (2) a detector-dependent readout increment, or (3) background shielding by large vehicles close to the RPM (also known as *ship-effect*. The first cause can be due to rainfall, which scavenges the radon progeny within clouds and causes its deposition on the ground [6]. The second cause can be determined by several factors, such as a decreased gain of the detector photomultiplier tube (PMT) due to an increase of the external temperature [7, 8, 9]. The gain decrease may result in an increase of the energy range corresponding to the selected detection window, and therefore in an increase of the overall count rate. In general, the temperature has multiple effects on a PMT operation, including dynode gain change and cathode sensitivity [10]. We recorded the detected background radiation and the environmental temperature to understand their correlation, and compensated for detector dependent effects, if necessary. The detector and PMT were in thermal equilibrium with the environment, therefore, it was possible to study the correlation between the measured temperature and the background count rate, directly. We did not include a temperature stabilization system, as done in some RPMs deployed in the field, because our objective was to investigate the effect of the temperature fluctuations in a relatively small range around room temperature on the readout.

We measured the background counts using a pair of 5.08 cm × 5.08 cm EJ-276 organic scintillators by Eljen Technologies. EJ-276 (4.546×10^{22} and 4.906×10^{22}, hydrogen and carbon atoms per cm^3, respectively) is a relatively new type of plastic scintillator, with pulse shape discrimination capability [11]. A 9214B PMT by Electron tubes converted the radiation-induced light pulses into current pulses. According to the manufacturer, the temperature coefficient of the PMT due to change in photocathode sensitivity and electron multiplier gain is -0.3%/°C [12]. The PMTs were connected to a desktop high-voltage power supply (CAEN DT5533EN) that supplied -1950 V to the first detector and -1838 V to the second one to gain match both the detectors at a pulse integral of 5.15 V ns/dt, corresponding to the Compton edge of a ^{137}Cs source, selected as the pulse integral corresponding to the 80% of the Compton edge with respect to its maximum. The lower detection threshold was 15 keVee. The detected pulses were digitized by a 14-bit 500-MSps CAEN DT5730 digitizer and acquired by the CAEN CoMPASS software [13]. Raw data were then processed using a custom software written in Matlab 2017, The MathWorks, Inc. Temperature and humidity measurements

were taken outdoor using a Teracom humidity and temperature sensor (TSH300v2) connected to a Teracom Ethernet data logger (TCW210-TH), precise to 0.1 °C, which was then connected via Ethernet to a lab computer for data storage. The data logger stored temperature and humidity measurements in 5 minute intervals.

2.2. Background, Temperature, and Humidity Data

Fig. 1a displays how the counts measurements changed over one week, from July 30 to August 6, 2020. The graph shows binned counts over five-minute intervals, with a variety of trends throughout the week. The large spikes in counts measurements align with rainfall events on their respective days. Data in selected time frames were used to create background spectra at four different background conditions, labeled in Fig. 1a as *stable*, *ramp*, *peak*, and *low*. The stable background was chosen at a time without any rainfall and relatively average temperature and humidity for the time of day, representing a baseline background level. Peak background corresponded with a time of heavy rainfall, creating a large spike in counts as expected. Ramp background corresponded with a time span when rain was beginning and the number of counts were rising to a peak region. Lastly, the low background region indicates a time span with the lowest number of recorded counts, also corresponding with low humidity for the time of day. These four regions are essential for analysis of how a changing background spectra and counts can interfere with the effectiveness of the unmixing algorithm. The main difference between the different background spectra can be noticed in Fig. 1b, with the *low* background being characterized by an overall lower intensity throughout the whole spectrum, compared to the other background spectra. Extended count gaps in Fig. 1a correspond to detector calibration periods. The calibration was performed by placing the Cesium-137 source in front of the detectors and checking that the shape and the Compton edge location were consistent with previous acquisitions.

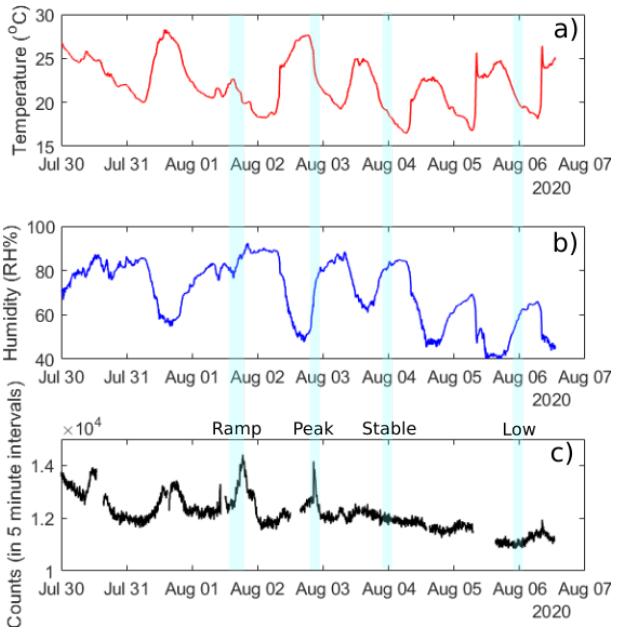

(a) Outdoor sensor data over time for a) Temperature, b) Humidity, and c) Counts. Ramp, Peak, Stable, and Low chosen regions are indicated with blue colored bars.

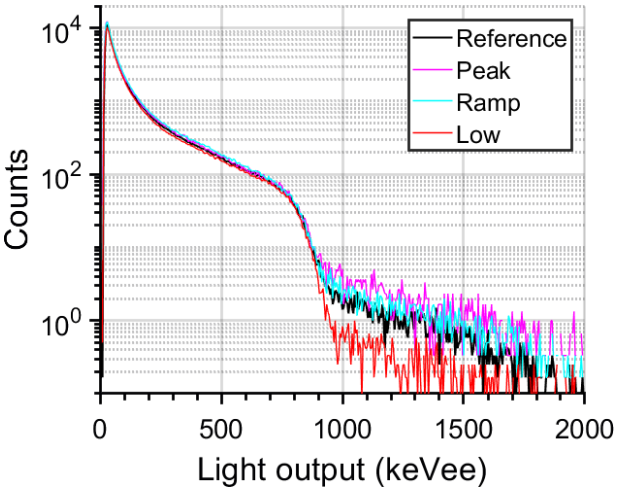

(b) Light Output background spectra measured under different conditions for one hour.

Figure 1: Background, Temperature, and Humidity Data

Figures 1a and 1b show how both the temperature and counts changed over the testing time period. As shown, the temperature had significant variation as a result of the varying high temperatures during the day, transitioning from night-to-day and day-to-night, and the sun's position relative to the detector. During the measurement, the temperature varied from 16.48°C to 28.28°C, with an average of 21.64°C. We analyzed the dependence of the background counts, in five-minute intervals, with the temperature to identify potential gain drifts caused by temperature gradients, and determine whether further spectrum re-calibration was necessary.

The sample standard deviation for counts in five minute intervals, σ, is approximately 588.7 counts, with some anomalies in recordings created by days of heavy rainfall. These anomalous results can be analyzed on a case-by-case basis, with most being a result of short bursts of heavy rainfall. At a temperature slightly above 20°C, a relatively high count rate was recorded due to a day of very heavy rainfall that caused an

increase in radioactivity from deposition of the radon progeny on the ground. Similarly, a region of low count rates (11,000 in five minutes, on average), and temperature ranging from 19°C to 24°C, was measured when the humidity was low. As expected, a positive weak correlation between count rate and temperature was found. The counts increased, on average, by about 1,600 from 16°C to 28°C, i.e., the temperature range of our experiment. This increment is comparable with 3σ of 1766.1. Therefore, we concluded that during the experiment the temperature negligibly affected the count rate. As such, all of the data collected can be used for applying to the unmixing algorithm without further spectral gain correction.

Fig. 2 shows the scatter-density plot of the measured counts as a function of the recorded humidity. The plot intensity is the frequency of occurrence of the counts. This plot shows a positive weak correlation between the count rate and the humidity, with a large concentration of points occurring around the 80-90 humidity range at around 12000 counts. Due to the higher humidities often corresponding to rainfall events, this positive weak correlation could also indicate a dependence of the counts on the occurrence of rainfall events. Many of the anomalous events occur in the high-count-high-humidity region of this plot, indicating many of these rainfall events happen at high humidity conditions, due to the increased chance of rainfall, and can cause a spike in the background radiation counts.

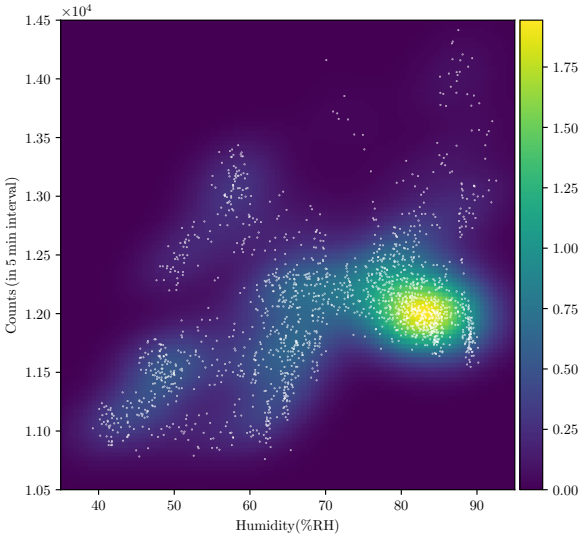

Figure 2: Counts as a function of Humidity Scatter Density Plot

2.3. Computational Methods for Neutron Source Identification

The detection of weapons-grade Plutonium isotopes is an essential role of the portal monitors, making the testing of this material with the algorithm useful to determine if it can be effectively identified. Because of this, our simulated standard neutron source is the 4.5 kg α-phase weapons-grade plutonium sphere, identified as the BeRP Ball [14]. This sphere can be simulated from the specifications given in [14], then shielded by a variety of common neutron shielding isotopes to create a spectra library of shielded plutonium. Identifying the presence of not only a strong neutron source, but also the type of shielding being used, can give operators a better understanding of the materials passing through the port of entry. The addition of both background and shielded spectra to the algorithm library allows for a more comprehensive spectral unmixing while maintaining the efficiency of the RPM scanning process.

The neutron spectra data gathering experiments made use of MCNPX-Polimi to simulate as close to the theoretical physical setup as possible. The neutron source being simulated was a 4.5 kg sphere of α-phase weapons-grade plutonium called a BeRP ball [14]. This source was created by Los Alamos National Laboratory in 1980, where 304 stainless steel cladding was added to the plutonium sphere. The BeRP ball source has an activity of 8.8 x 10^5 neutrons/second. This sphere consisted of various isotopes of plutonium, as well as a number of other elements in smaller proportions. With these specifications added into MCNP, a simulation setting up a physical shielding experiment could be done. In order to build out a library of possible shielding materials, four different shielding layer types were simulated at a distance of 40 cm away from the center of the BeRP ball source. The total combined thickness of the layers in each experiment was 2 inches, and the four orientations used were as follows: 2 inches Polyethylene, 2 inches Tungsten, 1 inch Depleted Uranium and 1 inch Polyethylene, and 1.5 inches Iron 0.5 inches Polyethylene. The detector that was simulated was a deuterated stilbene organic scintillation detector, with dimensions of 2x2x2 inches^3. Lastly, components of the physical setup, including an aluminum workbench and concrete flooring were added to make the simulation as close to the physical version of the experiment as possible. Each of the simulations was run with MCNPX-Polimi for a total of 20,000,000 source particles, corresponding to a 227.27 second physical experiment. This allows for the creation of an energy spectra spectra when exiting the shielding material and entering the detector, which can then be used as a spectral shape reference for the cross-section calculation method outlined in [5].

2.4. Radioisotope Library and Mixture Generation

We first generated a variety of gamma source radioisotope mixtures to test the effectiveness of the unmixing algorithm. The algorithm performance in identifying the present radionuclides and correctly estimating their fractions were calculated, as a function of the number of detected counts. These library spectra were measured using the same experimental setup as used for the background measurement. In this case, the acquisition was performed indoors. The isotope library included: ^{133}Ba, ^{109}Cd, ^{57}Co, ^{60}Co, ^{137}Cs, ^{54}Mn, ^{22}Na, and ^{238}U. Each source, except ^{238}U, had an activity of 1 μCi (3.7×10^4 Bq) as of October 19, 2017. The ^{238}U source was in the shape of a hollow rod coated by a 1.07-mm thick aluminum liner (2.54 cm outer diameter, 1 cm inner diameter and 25 cm length) of 1.8 Ci (6.66×10^{10} Bq) activity, measured on October 16, 2013. The measured spectra are displayed in Fig. 3. Each isotope was measured over a different time period, enough to collect approximately 2,000,000 counts in total. The light output was calibrated in electron-equivalent units using the Cs-137 Compton edge pulse integral value. The background of indoor measurements was not removed due its negligible scale compared to the radioisotope spectra counts. With these libraries created, the mixtures were then generated and used as input of the unmixing algorithm.

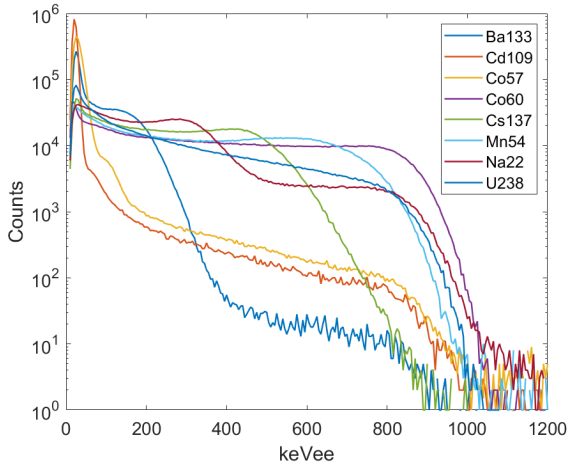

Figure 3: Library of radionuclides used for the unmixing algorithm, consisting of eight gamma-ray emitting isotopes.

We generated six different mixtures using the pulse integral spectra information from the library. These mixtures were chosen based on naturally occurring isotope combinations. Spectra with similar shapes but including different nuclides were also chosen to test the algorithm spectral sensitivity. Each mixture generation began by linearly combining the normalized spectra corresponding to the selected radionuclides scaled up the mixture counts level, followed by adding a set amount of stable reference background measurement, conservatively equivalent to one minute of detection time. Lastly, Poisson noise was added to each mixture to simulate Poisson noise in both the isotopic decay and background radiation. Each mixture was generated 100 times, with background and Poisson noise applied each time, and the unmixing algorithm was run over each iteration of the mixtures. The average value for predicted radionuclide relative amounts and probability of appearance was calculated from the unmixing algorithm iterations and reported in the heat maps in Fig. 6. This approach was then repeated for each of the varied amount of mixture counts (500, 1000, 5000, 10000, 25000, 50000, and 100000 not including background or Poisson noise). A stable background measurement was added to the library for the algorithm to achieve better results at lower count levels. The scale of typical vehicle RPM with four plastic scintillators may have a total background count rate of about 1000 gamma counts per second, with many alarms just being hundreds to thousands of gamma counts per second above background. These situations account for many of our lower count levels in the range, such as 500, 1000, and 5000 counts. The upper end of the count level range is included for better visualization, as well as including situations where higher count alarms do occur.

2.5. Shielding Material Library and Mixture Generation

Similar to the library for gamma radioisotopes, a library of spectra from a single neutron source with a variety of shielding materials was created. The materials used in the library were based on the four shielding configurations used in simulations, with each isotope in the library corresponding to one of the shielding layer types. For example, the polyethylene material is represented by the Carbon and Hydrogen isotopes in the library. The cross section of each material was used to perform the calculation as shown in equation 1, similar to that shown in [5]:

$$\phi_j^{mod} = W_j \prod_l \exp\left(-\sigma_{lj}\tau_l\right) \tag{1}$$

Equation 1 is used to represent how the BeRP Ball spectra is modified by the inclusion of the cross section and thickness data of the shielding material. In the equation, τ represents the 2 inch shielding thickness, l represents the material isotope, j represents the energy bin, σ_{lj} represents the cross section of

the material at a specific energy, and W_j represents the BeRP ball spectra at a specific energy group. This calculation produces a spectra that has been modified by the cross section of the shielding material. This calculation was then used for each shielding isotope to generate the library for the unmixing algorithm. These library spectra are shown in Fig. 4 below:

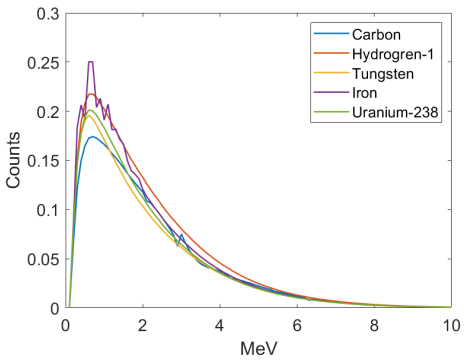

Figure 4: Library of shielding isotopes used for the unmixing algorithm, each modified with 2 inches of shielding material.

From these normalized spectra in Fig. 4, four different mixtures were generated to test the effectiveness of the unmixing algorithm in a similar manner to the gamma spectra mixtures. Poisson noise was added to each of the mixtures, along with having seven count levels for testing how few counts are needed so the algorithm can remain effective.

2.6. Unmixing Algorithm

As mentioned above, we used a Bayesian algorithm to find the mixing coefficients associated with each library nuclide to assess their contribution to the measured spectrum. In previous studies, we analyzed several Bayesian approaches to solve this problem [15, 4]. These methods exploit the posterior distribution of the mixing coefficients, by combining the observed data with available prior information. We have observed that a sparsity-promoting approach using a Bernoulli-truncated Gaussian (BTG) prior model yielded state-of-the-art estimates for the nuclide fractions in the unknown mixtures [4] and, therefore, we only consider this method in this work.

Given an observed light output spectrum $\mathbf{y} = [y_1, \ldots, y_M]^T$, observed in M energy bins, which is associated with a mixture of up to N known sources, whose individual spectral responses are denoted by $\{\mathbf{A}_{:,n}\}_{n=1,\ldots,N}$ and gathered in the $M \times N$ library matrix $\mathbf{A} = [\mathbf{A}_{:,1}, \ldots, \mathbf{A}_{:,N}] = [\mathbf{A}_{1,:}^T, \ldots, \mathbf{A}_{M,:}^T]^T$. Each $\mathbf{A}_{m,:}$ is a row vector gathering the spectral responses of the N known sources in the mth energy bin. The coefficient associated with the nth source, corresponding to the amount present in the mixture, is denoted by x_n and the N coefficients are gathered in the vector $\mathbf{x} = [x_1, \ldots, x_N]^T$. In this work, $N = 9$ since we included the eight library sources and a reference background spectrum, acquired over 12 hours and normalized to 1 (unit integral), like all the other library spectra. At a first approximation, we assume a linear mixing model of the source components, which can be expressed in matrix form as $\mathbf{y} \approx \mathbf{A}\mathbf{x}$. $\mathbf{A}$ is known and is omitted in all the conditional distributions hereafter. As mentioned above, the observation noise is modeled by Poisson noise, leading to the following form of the likelihood

$$f(y_m|\mathbf{x}) = (\mathbf{A}_{m,:}\mathbf{x})^{y_m} \exp\left[-\mathbf{A}_{m,:}\mathbf{x}\right]/y_m!, \quad \forall m = 1, \ldots, M. \tag{2}$$

The entries of $\mathbf{y}$ are independently distributed, i.e., $f(\mathbf{y}|\mathbf{x}) = \prod_{m=1}^{M} f(y_m|\mathbf{x}) = \prod_{m=1}^{M} f(y_m|\mathbf{A}_{m,:}\mathbf{x})$ and are conditioned on the value of $\mathbf{x}$. Bayesian methods rely on the knowledge of prior information available about $\mathbf{x}$, the coefficients, to enhance their recovery from the observable $\mathbf{y}$, the light output spectrum. The a-priori information is the prior distribution $f(\mathbf{x})$ and the estimation of $\mathbf{x}$ can then be achieved using the posterior distribution $f(\mathbf{x}|\mathbf{y}) = f(\mathbf{y}|\mathbf{x})f(\mathbf{x})/f(\mathbf{y})$.

The efficient sparsity-promoting BTG prior model of $\mathbf{x}$ is described in Eq. (3)

$$\begin{aligned} f(x_n|w_n) = (1 - w_n)\delta(x_n) + w_n\mathcal{N}_{\mathbb{R}^+}(x_n; 0, \sigma_n^2), \quad \forall n = 1, \ldots, N \\ f_n(w_n = 1) = \pi_n, \quad \forall n = 1, \ldots, N, \end{aligned} \tag{3}$$

In Eq.(3), $\delta(\cdot)$ denotes the Dirac delta function, which is equal to 1 when $x_n = 0$ and 0 elsewhere and where $\mathcal{N}_{\mathbb{R}^+}(x_n; 0, \sigma^2)$ is a probability density function (p.d.f.) truncated Gaussian distribution, defined on $\mathbb{R}^+$ to enforce the non-negativity of the elements of $\mathbf{x}$. The truncated Gaussian prior has hidden mean 0 and hidden variance σ^2these are the mean and variance of the non-truncated Gaussian distribution). The

presence of the nth source is controlled by the binary variable w_n, which is equal to 1 when the nth is present and 0 otherwise. π_n is the prior probability of presence of the nth source.

We set $\pi_n = 1/N, \forall n$ as we expect a limited number of sources to be simultaneously present in the mixture, while we do not wish to promote any specific source. These parameters can however modified by the practitioners. We set the variances $\{\sigma_n^2\}$ as in Eq. (4) for each source

$$\sigma_n^2 = 0.1 \sum_{m=1}^{M} y_m. \tag{4}$$

Instead of considering a prior model only for $\mathbf{x}$, Eq. 3 defines a joint prior model for $(\mathbf{x}, \mathbf{w})$, where $\mathbf{w} = [w_1, \ldots, w_N]^T$, expressed as $f(\mathbf{x}, \mathbf{w}) = \prod_{n=1}^{N} f(x_n|w_n) f_n(w_n)$. The proposed unmixing algorithm thus aims at estimating jointly $(\mathbf{x}, \mathbf{w})$, i.e., at performing jointly the source identification (through $\mathbf{w}$) and quantification (through $\mathbf{x}$).

Using the Bayes' rule, the joint posterior distribution of $(\mathbf{x}, \mathbf{w})$ is given by $f(\mathbf{x}, \mathbf{w}|\mathbf{y}) = f(\mathbf{y}|\mathbf{x}) f(\mathbf{x}, \mathbf{w}) / f(\mathbf{y})$.

The algorithm adopted in this paper and originally described in [4] relies on approximate Bayesian estimation and builds an approximate distribution $Q(\mathbf{x}, \mathbf{w}) \approx f(\mathbf{x}, \mathbf{w}|\mathbf{y})$ whose moments are much simpler to evaluate than those of $f(\mathbf{x}, \mathbf{w}|\mathbf{y})$. The method belongs to the so-called class of expectation propagation (EP) methods [16] to provide approximate point estimates of the mean and the covariance of the posterior distribution of $\mathbf{x}$ (and $\mathbf{w}$). It offers several advantages compared to traditional approaches that exploit the posterior distribution using Hamiltonian Monte Carlo methods [15, 17] and is also motivated by the fact that the posterior means $E_{f(\mathbf{x},\mathbf{w}|\mathbf{y})}[\mathbf{x}]$ and $E_{f(\mathbf{x},\mathbf{w}|\mathbf{y})}[\mathbf{w}]$ associated with the posterior distribution $f(\mathbf{x}, \mathbf{w}|\mathbf{y})$ are intractable analytically. Further details on the EP algorithm and its implementation can be found in our previous work [4] and are available online in its current version at [18].

2.7. Unmixing Algorithm Classification Methodology

In order to determine the effectiveness of the unmixing algorithm, 100 iterations of the chosen mixtures were generated and run through the algorithm to generate two outputs: 1) The predicted proportional amounts of each radioisotope or shielding material for each of the mixtures, and 2) The predicted probability, ranging from 0 to 1, of the presence of each radioisotope or shielding material in the mixture. These iterations were performed for a variety of count levels, ranging from 500 total counts for each spectra up to 100,000 counts. These values are then used for the creation of the heat maps shown in Figures 6 and 7 by using an average calculation for the 100 iterations. These heat maps show the average presence probabilities for each isotope or shielding material at each mixture counts level, with the color bar representing this 0 to 1 numerical information on a color scale. These probabilities allow for the analysis of the unmixing algorithm's effectiveness at low and high count levels, with the case of low count levels achieving high predicted probabilities on the correct isotopes and materials being ideal for showing the algorithm's ability in a realistic portal monitor situation.

3. Results

3.1. Source Identification - Gamma

The source identification for gamma source radioisotopes uses the 100 algorithm runs of each of the mixtures to average the predicted probability of which radioisotopes are present in the mixture. Because many of these sources can be low activity, and the time scale of the portal monitor passing is very short, the algorithm should be able to correctly identify which isotopes are present at a low total number of counts to be considered effective. In order to make this possible, we found that the inclusion of background spectra in the library was necessary as shown in Figures 5 and 6:

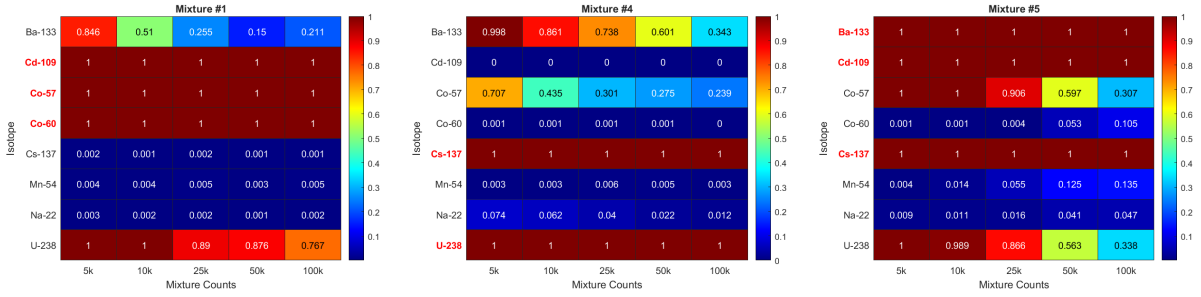

(a) Mixture #1 Heat Map (b) Mixture #4 Heat Map (c) Mixture #5 Heat Map

Figure 5: Heat Maps of three tested mixtures when background is NOT included in the library. Materials highlighted in red indicate the present materials in each mixture. Each number represents the average predicted probability of the individual isotope being present.

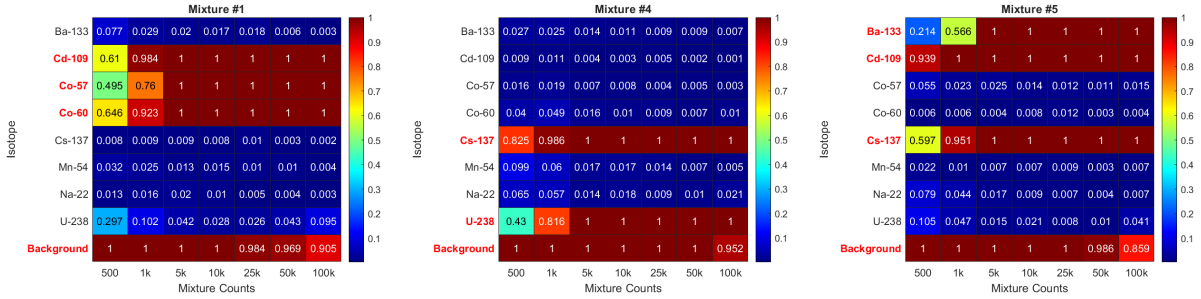

(a) Mixture #1 Heat Map (b) Mixture #4 Heat Map (c) Mixture #5 Heat Map

Figure 6: Heat Maps of three tested mixtures when background is included in the library. Materials highlighted in red indicate the present materials in each mixture. Each number represents the average predicted probability of the individual isotope being present.

Comparing the effectiveness of the algorithm when the background is included in the library to when it is not included shows how the background included results allow for accurate source identification at a significantly lower counts level. The algorithm is able to consistently identify the presence of the background and is able to factor it out of the identification of other sources, therefore improving how many counts are needed in order to separate the source spectra. Similarly, isotopes such as ^{238}U had spectra that were very similar to the background spectra and therefore were often identified as being present until very high count levels were tested. With background included, the algorithm was able to determine the difference between these spectra at relatively low count levels.

3.2. Source Identification - Neutron

The source identification of neutron shielded sources occurred through the creation of shielding material mixtures and combinations that were similarly done in MCNPX-Polimi simulation. Using the cross section method outlined above, three mixtures were created using low-Z and high-Z materials to simulate possible shielding scenarios, with a fourth mixture testing two high-Z materials. After the generation of 100 iterations of the mixtures and running them through the unmixing algorithm, the following heat maps were created for these shielding scenarios in Fig. 7:

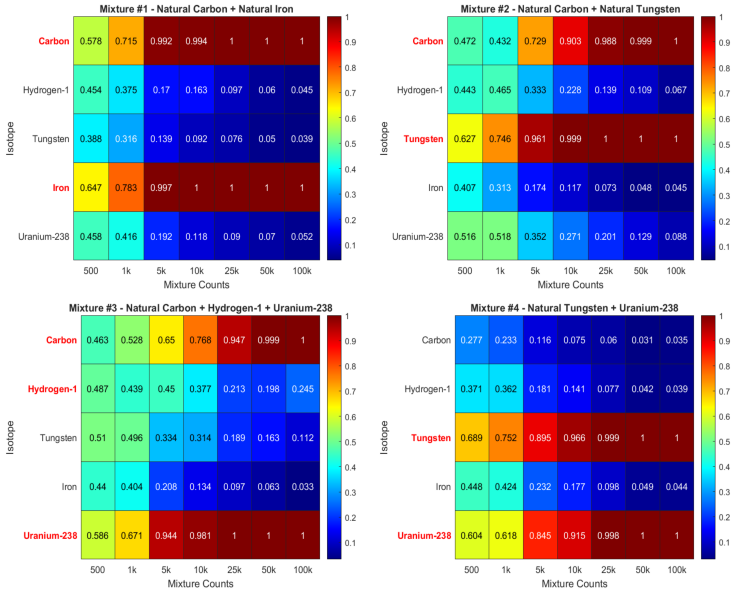

Figure 7: Heat maps of each of the four mixtures of different shielding materials with the fixed BeRP Ball neutron source. Materials highlighted in red indicate the present materials in each mixture.

As shown in the heat maps in Fig. 7, the algorithm's certainty on the presence of the correct isotopes vastly increases as more counts are included in the mixture. Unlike the gamma radioisotope mixtures, many of these shielding mixtures are not identified with a certainty of over 50% until reaching about 5000 counts in the mixture. This is likely due to the cross section modification to the BeRP ball spectra making these shielding material spectra all very similar in shape and scale, thus causing more counts to be needed for a differentiation to be made by the algorithm.

4. Discussion and Conclusions

We demonstrated that Bayesian unmixing algorithms can be a viable, computationally cost-effective approach to identify the types of radioactive materials in transit through RPMs [4]. The overall RPM sensitivity and false alarm rate depends mostly on the detectors' intrinsic efficiency and geometric solid angle with respect to the source [3]. However, when an alarm is reported, the correct identification of SNMs is crucial to discriminate them from other sources, such as NORM or radionuclides for medical use. While the minimum detectable amount of radioactivity strongly depends on system parameters, the identification performance directly depends on the unmixing algorithm and the detectors' energy resolution [4]. RPM performances in the field are strongly affected by changes in the radiation background, which could be due to surrounding materials or to transient atmospheric conditions. We first focused on the latter problem and tested the performance of our unmixing algorithm at different background conditions. We used plastic organic scintillators to monitor the radiation background and selected background spectra during different time periods during an outdoor continuous measurement. After identifying a reference background, we have selected the background spectra corresponding to a rapidly increasing count rate, to a count rate peak, and to a count rate significantly lower than the reference. The selected background spectra mainly differed in terms of intensity, but a spectral increase in the high energy region was also found, in the presence of heavy rain, which is consistent with our expectations. The reference background should be included in the library of radionuclides, as it is expected to be present at all times. We tested the unmixing algorithm when the different background spectra were added to the mixture of radionuclides, instead of the reference background. We found that the capability of identifying the nuclides present in the mixture was not significantly affected by the presence of a background other than the reference one. We found a root-mean-square error between the true mixture fractions and the estimated ones of approximately 1.4%, regardless of the type of background used, when 100,000 counts were detected. As the number of counts decreased, the RMSE increased and a slight sensitivity to the background type was observed at 500 counts. At low count regimes, not only the estimated mixture fractions can deviate from the true ones but nuclides can also be misidentified. Nonetheless, the unmixing algorithm provides an inherent uncertainty measure that can be used to determine whether a longer acquisition, with a higher signal-to-noise ratio is needed. We can conclude that the developed unmixing algorithm is robust against background changes that may occur because of varying atmospheric conditions within the 16 °C - 28 °C range. While this is not

a temperature range found in harsh environments, it could be easily experienced inside an enclosure with coarse temperature control.

Applying the unmixing algorithm to the different shielding isotopes yields similarly effective results to the gamma isotope unmixing. The algorithm is able to effectively differentiate between these very similar library spectra when achieving about 5000 total counts in the mixture spectra. Although a greater number of pulses are needed to reliably identify the correct mixture isotopes when compared to the gamma isotope unmixing, the relative strength of the neutron sources allow for this higher number of detected counts in the same RPM scanning time. Future work can be done to expand the library to more shielding components, as well as using physical detected data from SNM and shielded SNM to generate the shielding material spectra library rather than simulated data. Work is being done to analyze detected data from the unshielded BeRP Ball, along with several shielded BeRP Ball configurations, and apply these to the unmixing algorithm in the same manner to that performed in the discussed simulations. Additionally, future work can be done to account for the gain drift of the RPM detectors over time by incorporating a gain-dependent parameter in the library. This would allow for the algorithm to remain accurate without recalibrating the RPM detectors as the gain drifts over time.

Acknowledgments

This work was funded in part by the Nuclear Regulatory Commission Faculty Development Grant number 31310019M0011 and the Consortium for Verification Technology under Department of Energy National Nuclear Security Administration award number DE-NA0002534. This work was also supported by the Royal Academy of Engineering under the Research Fellowship scheme RF201617/16/31 and by the Engineering and Physical Sciences Research Council (EPSRC) Grant number EP/S000631/1 and the MOD University Defence Research Collaboration (UDRC) in Signal Processing.

References

[1] R. T. Kouzes, J. H. Ely, B. D. Geelhood, R. R. Hansen, E. A. Lepel, J. E. Schweppe, E. R. Siciliano, D. J. Strom, R. A. Warner, Naturally occurring radioactive materials and medical isotopes at border crossings, in: IEEE Nuclear Science Symposium Conference Record, 2003.

[2] Department of Homeland Security, Portable Radiation Portal Monitors Market Survey Report (2015).
URL https://www.dhs.gov/sites/default/files/publications/PortRadPortalMons-MSR_0315-508.pdf

[3] M. G. Paff, S. D. Clarke, S. A. Pozzi, Organic liquid scintillation detector shape and volume impact on radiation portal monitors, Nuclear Instruments and Methods in Physics Research, Section A: Accelerators, Spectrometers, Detectors and Associated Equipment (2016). doi:10.1016/j.nima.2016.03.102.

[4] Expectation-propagation for weak radionuclide identification at radiation portal monitors, Scientific Reports (2020). doi:10.1038/s41598-020-62947-3.

[5] C. C. Lawrence, M. Febbraro, M. Flaska, S. A. Pozzi, F. D. Becchetti, Warhead verification as inverse problem: Applications of neutron spectrum unfolding from organic-scintillator measurements, Journal of Applied Physics 120 (6) (2016) 064501. arXiv:https://doi.org/10.1063/1.4960131, doi:10.1063/1.4960131.
URL https://doi.org/10.1063/1.4960131

[6] R. J. Livesay, C. S. Blessinger, T. F. Guzzardo, P. A. Hausladen, Rain-induced increase in background radiation detected by Radiation Portal Monitors, Journal of Environmental Radioactivity (2014). doi:10.1016/j.jenvrad.2014.07.010.

[7] P. L. Wang, Y. L. Zhang, Z. Z. Xu, X. L. Wang, Study on the temperature dependence of BGO light yield, Science China: Physics, Mechanics and Astronomy (2014). doi:10.1007/s11433-014-5548-4.

[8] D. Gehman, M. Smith-Nelson, K. Ianakiev, D. Dinwiddie, B. Rooney, Temperature dependency analysis of light output from an NE-213 liquid scintillator, in: IEEE Nuclear Science Symposium Conference Record, 2007. doi:10.1109/NSSMIC.2007.4437269.

[9] S. H. Liebson, J. W. Keller, The temperature dependence of organic scintillation counters [23] (1950). doi:10.1103/PhysRev.78.305.

[10] Hamamatsu Photonics, Mcp-Pmt, Tech. rep. (2007).

[11] Eljen Technology, PULSE SHAPE DISCRIMINATION EJ-276 and EJ-276G.
URL https://eljentechnology.com/products/plastic-scintillators/ej-276

[12] Hamamatsu Photonics, 9214b pmt specification sheet (2007).

[13] CAEN S.pA., CoMPASS Multiparametric DAQ Software for Physics Applications.

[14] J. K. Mattingly, Polyethylene-reflected plutonium metal sphere : subcritical neutron and gamma measurements. (11 2009). doi:10.2172/974870.
URL https://www.osti.gov/biblio/974870

[15] M. Paff, A. D. Fulvio, Y. Altmann, S. D. Clarke, A. O. Hero, S. A. Pozzi, Identification of mixed sources with an organic scintillator-based radiation portal monitor, Journal of Nuclear Materials Management 46 (4) (2018) 48–57.

[16] T. P. Minka, Expectation propagation for approximate bayesian inference, in: Proceedings of the Seventeenth conference on Uncertainty in artificial intelligence, Morgan Kaufmann Publishers Inc., 2001, pp. 362–369.

[17] A. Vehtari, A. Gelman, T. Sivula, P. Jylänki, D. Tran, S. Sahai, P. Blomstedt, J. P. Cunningham, D. Schiminovich, C. Robert, Expectation propagation as a way of life: A framework for bayesian inference on partitioned data (2014). arXiv:1412.4869.
URL https://arxiv.org/abs/1412.4869v4

[18] Yoann Altmann, Sparse Unmixing Poisson Noise EP.
URL https://gitlab.com/yaltmann/sparse_unmixing_poisson_noise_ep